

The Polish doughnuts revisited

I. The angular momentum distribution and equipressure surfaces

Qian Lei^{1,2}, Marek A. Abramowicz^{1,3}, P. Chris Fragile^{4,1}, Jiří Horák^{5,1}, Mami Machida⁶, and Odele Straub^{3,1}

¹ Department of Physics, Göteborg University, SE-412-96 Göteborg, Sweden
e-mail: Marek.Abramowicz@physics.gu.se

² Department of Astronomy, Peking University Cheng Fu St. 209, 100871 Beijing, China*
e-mail: qianlivan@gmail.com

³ N. Copernicus Astronomical Center, Polish Academy of Sciences, Bartycka 18, 00-716 Warszawa, Poland
e-mail: odele@camk.edu.pl

⁴ Physics & Astronomy College of Charleston, 58 Coming Street Charleston SC 29424, U.S.A.
e-mail: FragileP@cofc.edu

⁵ Astronomical Institute, Academy of Sciences of the Czech Republic, Boční II/1401a, 141-31 Prague, Czech Republic
e-mail: jiri.horak@cdsw.cz

⁶ National Astronomical Observatory of Japan 2-21-1 Osawa, Mitaka, 181-8588 Tokyo, Japan
e-mail: mami@th.nao.ac.jp

Received ???; accepted ???

ABSTRACT

We construct a new family of analytic models of black hole accretion disks in dynamical equilibria. Our construction is based on assuming distributions of angular momentum and entropy. For a particular choice of the distribution of angular momentum, we calculate the shapes of equipressure surfaces. The equipressure surfaces we find are similar to those in thick, slim and thin disks, and to those in ADAFs.

Key words. black holes – accretion disks – analytic models

1. Introduction

In accretion disk theory one is often interested in phenomena that occur on a “dynamical” timescale \mathcal{T}_0 much shorter than the “viscous” timescale $\mathcal{T}[\mathcal{L}]$ needed for angular momentum redistribution and the “thermal” timescale $\mathcal{T}[\mathcal{S}]$ needed for entropy redistribution¹,

$$\mathcal{T}_0 \ll \min(\mathcal{T}[\mathcal{L}], \mathcal{T}[\mathcal{S}]). \quad (1)$$

The question whether it is physically legitimate to approximately describe the black hole accretion flows (at least in some “averaged” sense) in terms of stationary (independent on t) and axially symmetric (independent on ϕ) dynamical equilibria, is not yet resolved. While observations seem to suggest that many real astrophysical sources experience periods in which this assumption is quite reasonable, several authors point out that the results of recent numerical simulations seem to indicate that the MRI and other instabilities make the black hole accretion flows genuinely non-steady and non-symmetric, and that the very concept of the separate timescales (1) may be questionable in the sense that locally $\mathcal{T}_0 \approx \mathcal{T}[\mathcal{L}] \approx \mathcal{T}[\mathcal{S}]$. However, this assumption has been made in *all* existing comparisons between the-

ory and observations, be they by detailed spectral fitting (e.g. Shafee & al. 2007, 2008, and references there), line profile fitting (e.g. Fabian & Vaughan 2003), or studying small amplitude oscillations (see Abramowicz 2005, for references). It seems that the present understanding of the black hole accretion phenomenon rests, in a major way, on studies of stationary and axially symmetric models.

From the point of view of mathematical self-consistency, in modeling of these stationary and axially symmetric dynamical equilibria, distributions of the *conserved* angular momentum and entropy,

$$\ell = \ell(\xi, \eta), \quad s = s(\xi, \eta), \quad (2)$$

may be considered as being *free functions* of the Lagrangian coordinates (Ostriker & al. 1966; Abramowicz 1970; Bardeen 1970). The Lagrangian coordinates ξ, η are defined by demanding that a narrow ring of matter $(\xi, \xi + d\xi), (\eta, \eta + d\eta)$ has the rest mass $dM_0 = \rho_0(\xi, \eta)d\xi d\eta$ with ρ_0 being the rest mass density. In the full physical description, the form of the functions in (2) is not arbitrary but given by the dissipative processes, like viscosity and radiative transfer. At present, several important aspects of these processes are still unknown, so there is still no practical way to calculate physically consistent models of accretion flows from first principles, without involving some ad hoc assumptions, or neglecting some important processes. Neither the hydrodynamical simulations (that e.g. use the ad hoc $\alpha = \text{const}$ viscosity prescription), nor the present day MHD simulations (that e.g. neglect radiative transfer) could be considered satisfactory. Furthermore, the simplifications made in these simulations

* permanent address

¹ We use the spherical Boyer-Lindquist coordinates t, ϕ, r, θ , the geometrical units $c = 1 = G$ and the $+$ $-$ $-$ signature. The Kerr metric is described by the “geometrical” mass M and the “geometrical” spin parameter $0 < a < 1$, that relate to the “physical” mass and angular momentum by the rescaling, $M = GM_{\text{phys}}/c^2$, $a = J_{\text{phys}}/(Mc)$. Partial derivatives are denoted by ∂_i and covariant derivatives by ∇_i .

are mathematically equivalent to guessing free functions (such as the entropy distribution). Bohdan Paczyński pointed out that it could often be more pragmatic to make a physically motivated guess of the final result, e.g. to guess the form of the angular momentum and entropy distributions.

In practice, it is far easier to guess and use the coordinate distributions of the *specific* angular momentum and entropy,

$$\mathcal{L} = \mathcal{L}(r, \theta), \quad (3)$$

$$S = S(r, \theta), \quad (4)$$

than the Lagrangian distributions (2). However, one does not know a priori the relation between the conserved ℓ and specific \mathcal{L} angular momenta (and entropy), or the functions, $\xi = \xi(r, \theta)$, $\eta = \eta(r, \theta)$. Thus, assuming (3) and (4) is not equivalent to assuming (2), and usually it should be a subject to some consistency conditions. We shall return to this point in Section 6.

In several “astrophysical scenarios” one indeed guesses a particular form of (3) and (4). For example, the celebrated Shakura & Sunyaev (1973) *thin disk* model assumes the Keplerian distribution of angular momentum,

$$\mathcal{L}(r, \theta) = \mathcal{L}_K(r) \equiv \frac{M^{1/2} (r^2 - 2aM^{1/2}r^{1/2} + a^2)}{r^{3/2} - 2Mr^{1/2} + aM^{1/2}}, \quad (5)$$

and the popular *cold-disk-plus-hot-corona* model assumes a low entropy flat disk surrounded by high entropy, more spherical corona. These models contributed considerably to the understanding of black-hole accretion physics.

The mathematically simplest assumption for the angular momentum and entropy distribution is, obviously,

$$\mathcal{L}(r, \theta) = \mathcal{L}_0 = \text{const}, \quad (6)$$

$$S(r, \theta) = S_0 = \text{const}. \quad (7)$$

This was used by Paczyński and his Warsaw team to introduce the *thick disk* models (Abramowicz & al. 1978; Kozłowski & al. 1978; Jaroszyński & al. 1980; Paczyński & Wiita 1980; Abramowicz & al. 1981; Abramowicz 1981; Paczyński 1982). Thick disks have characteristic toroidal shapes, resembling a doughnut. Probably for this reason, Martin Rees coined the name of *Polish doughnuts*² for them.

Figure 1 shows a comparison of a state-of-art MHD simulation of black-hole accretion (time and azimuth averaged) with a Polish doughnut corresponding to a particular \mathcal{L}_0 . Both models show the same characteristic features of black hole accretion: (i) a funnel along the rotation axis, relevant for jet collimation and acceleration; (ii) a pressure maximum, possibly relevant for epicyclic oscillatory modes; and (iii) a cusp-like self-crossing of one particular equipressure surface, relevant for an inner boundary condition, and for stabilization of the Papaloizou-Pringle (Blaes 1987), thermal, and viscous instabilities (Abramowicz 1971). The cusp is located between the radii of marginally stable and marginally bound circular orbits,

$$r_{mb} < r_{cusp} < r_{ms} \equiv \text{ISCO}. \quad (8)$$

Polish doughnuts have been useful in semi-analytic studies of the astrophysical appearance of super-Eddington accretion (see e.g. Sikora 1971; Madau 1988; Szuszkiewicz & al. 1996) and in analytic calculations of small-amplitude oscillations of accretion structures in connection with QPOs (see e.g. Blaes & al.

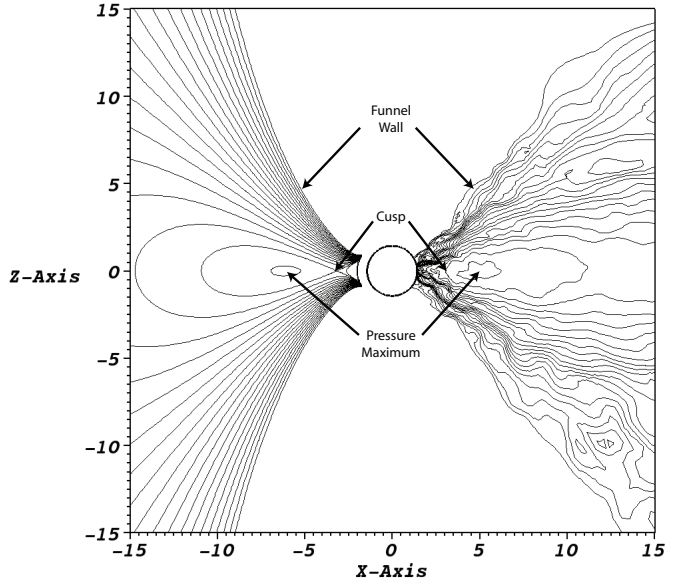


Fig. 1. Equipressure surfaces in a very simple and analytic Polish doughnut (left, with linear spacing), and a sophisticated, state-of-art full 3D MHD numerical simulation (right, with logarithmic spacing). Although the shapes of equipressure surfaces are remarkably similar, in the numerical model the pressure gradient is seriously larger, and visibly enhanced along roughly conical surfaces, approximately 30° from the equatorial plane. (Figure taken from Abramowicz & Fragile 2008)

2006). In the same context, numerical studies of their oscillation properties for different angular momentum distributions were first carried out by Rezzolla & al. (2003a,b). Moreover, Polish doughnuts are routinely used as convenient starting initial configurations in numerical simulations (e.g. Hawley et al. 2001; De Villiers & Hawley 2003). Recently, Komissarov (2006) has constructed analytic models of magnetized Polish doughnuts. However, a closer inspection of Figure 1 reveals that the numerically constructed model of accretion has a (much) larger “vertical” pressure gradient than the analytic Polish doughnut, and that in the numerical model the gradient is visibly enhanced along roughly conical surfaces, approximately 30° from the equatorial plane. This (and several other) detailed features of the accretion structure cannot be modeled by either the Keplerian nor the constant angular momentum assumption alone. We suggest and discuss in this paper a simple but flexible ansatz, that is a combination of the two standard distributions, Keplerian (5) and constant (6). The new ansatz preserves the virtues of assuming the standard distributions where this is appropriate, but leads to a far richer variety of possible accretion structures, as are indeed seen in numerical simulations.

2. Assumptions and definitions

We assume that the accretion flow is stationary and axially symmetric. This assumption expressed in terms of the Boyer-Lindquist spherical coordinates states that the flow properties depend only on the radial and polar coordinates r, θ , and are independent on time t and azimuth ϕ . We also assume that the dynamical timescale is much shorter than the thermal and vis-

² However, real Polish doughnuts (called *paczki* in Polish) have spherical shapes. They are definitely non-toroidal — see e.g. <http://en.wikipedia.org/wiki/Paczki>.

cus ones (1). Accordingly, we ignore dissipation and assume the stress-energy tensor in the perfect fluid form,

$$T^i_k = (p + \epsilon)u^i u_k - p\delta^i_k, \quad (9)$$

with p and ϵ being the pressure and energy density, respectively. The four velocity of matter u^i is assumed to be purely circular,

$$u^i = (u^t, u^\phi, 0, 0). \quad (10)$$

The last assumption is not fulfilled close to the cusp (see Figure 1), where there is a transition from “almost circular” to almost “free-fall” radial trajectories. Nevertheless, the transition could be incorporated in the form of the inner boundary condition (the relativistic Roche lobe overflow, see e.g. Abramowicz 1985).

One introduces the specific angular momentum \mathcal{L} , the angular velocity Ω , and the redshift factor A by the well known and standard definitions,

$$\mathcal{L} = -\frac{u_\phi}{u_t}, \quad \Omega = \frac{u^\phi}{u^t}, \quad A^{-2} = g_{tt} + 2\Omega g_{t\phi} + \Omega^2 g_{\phi\phi}. \quad (11)$$

The specific angular momentum and angular velocity are linked by

$$\mathcal{L} = -\frac{\Omega g_{\phi\phi} + g_{t\phi}}{\Omega g_{t\phi} + g_{tt}}, \quad \Omega = -\frac{\mathcal{L} g_{tt} + g_{t\phi}}{\mathcal{L} g_{t\phi} + g_{\phi\phi}}. \quad (12)$$

The conserved angular momentum ℓ is given by,

$$\ell = \frac{(p + \epsilon)u_t}{\rho_0} \mathcal{L}. \quad (13)$$

3. The shapes of the equipressure surfaces

In this section we briefly discuss one particularly useful result obtained by Jaroszyński & al. (1980). It states that for a perfect fluid matter rotating on circular trajectories around a black hole, the shapes and location of the equipressure surfaces $p(r, \theta) = \text{const}$ follow directly from the assumed angular momentum distribution (3) alone. In particular, they are independent of the equation of state, $p = p(\epsilon, \mathcal{S})$, and the assumed entropy distribution (4).

For a perfect-fluid matter, the equation of motion $\nabla_i T^i_k = 0$ yields,

$$\frac{\partial_i p}{p + \epsilon} = -\frac{1}{2} \frac{\partial_i g^{tt} - 2\mathcal{L} \partial_i g^{t\phi} + \mathcal{L}^2 \partial_i g^{\phi\phi}}{g^{tt} - 2\mathcal{L} g^{t\phi} + \mathcal{L}^2 g^{\phi\phi}}, \quad (14)$$

which may be transformed into,

$$\frac{\partial_i p}{p + \epsilon} = \partial_i \ln A + \frac{\mathcal{L} \partial_i \Omega}{1 - \mathcal{L} \Omega} \quad (15)$$

From the second derivative commutator $\partial_r \partial_\theta - \partial_\theta \partial_r$ of the above equation,

$$\frac{\partial_r p \partial_\theta \epsilon - \partial_\theta p \partial_r \epsilon}{(p + \epsilon)^2} = \frac{\partial_r \Omega \partial_\theta \mathcal{L} - \partial_\theta \Omega \partial_r \mathcal{L}}{(1 - \mathcal{L} \Omega)^2}, \quad (16)$$

one derives (see e.g. Abramowicz 1971) the von Zeipel condition: $p(r, \theta) = \text{const}$ surfaces coincide with those of $\epsilon(r, \theta) = \text{const}$, if and only if the surfaces $\mathcal{L}(r, \theta) = \text{const}$ coincide with those $\Omega(r, \theta) = \text{const}$ ³. Obviously, the constant angular momentum case satisfies the von Zeipel condition.

³ The best known Newtonian version of the von Zeipel condition states that for a barytropic fluid $p = p(\epsilon)$, both angular velocity and angular momentum are constant on cylinders, $\Omega = \Omega(R)$, $\mathcal{L} = \mathcal{L}(R)$, with $R = r \sin \theta$ being the distance from the rotation axis.

Jaroszyński & al. (1980) have also discussed a general, non barytropic case. They wrote equation (14) twice, for $i = r$ and $i = \theta$, and divided the two equations side by side to get

$$\frac{\partial_r p}{\partial_\theta p} = \frac{\partial_r g^{tt} - 2\mathcal{L} \partial_r g^{t\phi} + \mathcal{L}^2 \partial_r g^{\phi\phi}}{\partial_\theta g^{tt} - 2\mathcal{L} \partial_\theta g^{t\phi} + \mathcal{L}^2 \partial_\theta g^{\phi\phi}} \equiv -F(r, \theta). \quad (17)$$

For the Kerr metric components one knows the functions $g^{ik} = g^{ik}(r, \theta)$, and therefore the function $F(r, \theta)$ in the right hand side of (17) is known explicitly in terms of r and θ , if one knows or assumes the angular momentum distribution $\mathcal{L} = \mathcal{L}(r, \theta)$. This has an important practical consequence.

Let $\theta = \theta(r)$ be the explicit equation for the equipressure surface $p(r, \theta) = \text{const}$. It is, $d\theta/dr = -\partial_r p / \partial_\theta p$. If the function $F(r, \theta)$ in (17) is known, then equation (17) takes the form of an ordinary differential equation for the equipressure surface, $\theta = \theta(r)$,

$$\frac{d\theta}{dr} = F(r, \theta), \quad (18)$$

with the explicitly known right hand side. It may be therefore directly integrated to get all the possible locations for the equipressure surfaces.

4. The angular momentum distribution

4.1. Physical arguments: the radial distribution

Jaroszyński & al. (1980) discussed general arguments showing that the slope of the specific angular momentum should be between two extreme: the slope corresponding to $\mathcal{L} = \text{const}$ and the slope corresponding to $\Omega = \text{const}$. These two cases, together with the Keplerian one $\mathcal{L} = \mathcal{L}_K$, may be considered as useful archetypes in discussing arguments relevant to the angular momentum distribution.

Indeed, far away from the black hole $r \gg r_G$, these arguments are well known (see e.g. Frank & al. 2002) and together with numerous numerical simulations show that typically (i.e. in a stationary case with no shocks) the specific angular momentum should be slightly sub-Keplerian $\mathcal{L}(r, \pi/2) \approx \mathcal{L}_K(r)$. There is a solid consensus on this point.

The situation close to the black hole is less clear because there is not sufficient knowledge of the nature of the stress operating in the innermost part of the flow, i.e. approximately between the horizon and the ISCO. Formally, one may consider two extreme ideal cases, depending whether the stress is very small or very large.

In the first case, the almost vanishing stress implies that the fluid is almost free-falling, and therefore the angular momentum is almost constant along fluid lines. This leads to $\mathcal{L}(r, \pi/2) \approx \text{const}$. Such situation is typical for the thin Shakura & Sunyaev (1973) and slim (Abramowicz & al. 1988) accretion disks. In the second case, one may imagine a powerful instability like MRI, which occurs when $d\Omega/dr \neq 0$. It may force the fluid closer to the marginally stable state $\Omega = \text{const}$. This situation may be relevant for ADAFs (Narayan & Yi 1988; Abramowicz & al. 1995).

4.2. The new ansatz

We suggest adopting the following assumption for the angular momentum distribution,

$$\mathcal{L}(r, \theta) = \begin{cases} \mathcal{L}_0 \left(\frac{\mathcal{L}_K(r)}{\mathcal{L}_0} \right)^\beta \sin^{2\gamma} \theta & \text{for } r \geq r_{ms} \\ \mathcal{L}_{ms}(r) \sin^{2\gamma} \theta & \text{for } r < r_{ms} \end{cases} \quad (19)$$

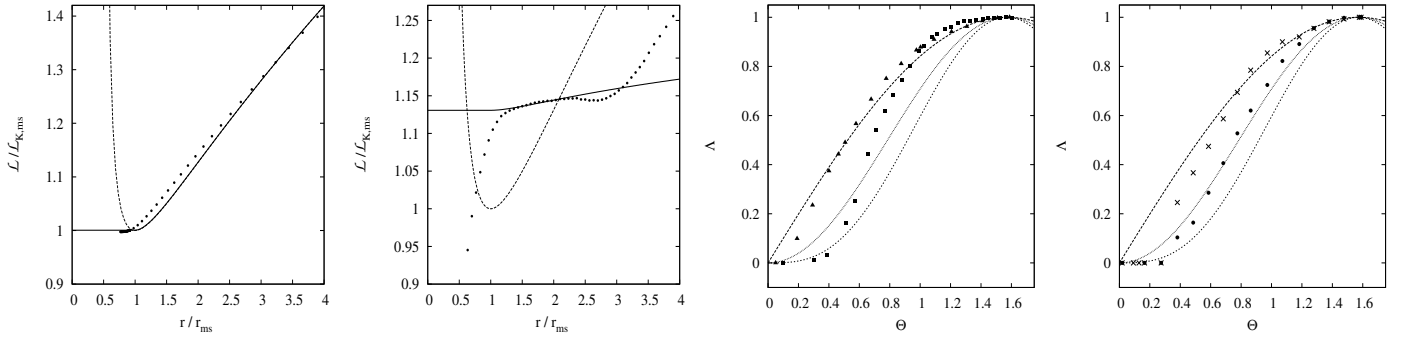


Fig. 2. (a) and (b): the distribution of angular momentum on the equatorial plane. Thick lines correspond to the angular momentum predicted by our analytic formula, dashed lines show the Keplerian angular momentum distribution and dots to the simulation data. (a): Kerr geometry $a = 0.9$ simulations by Sądowski (2008). (b): Pseudo-Newtonian MHD simulations by Machida & Matsumoto (2008). (c) and (d): angular momentum off the equatorial plane, normalized to its equatorial plane value, $\Lambda = \mathcal{L}(r, \theta)/\mathcal{L}(r, \pi/2)$. Lines correspond to the $\sin^{2\gamma} \theta$ distribution at $r = 10r_G$: long-dashed $\gamma = 0.5$, dotted $\gamma = 1.0$, and short dashed $\gamma = 1.5$. Points are taken from time-dependent, fully 3-D, MHD numerical simulations. They correspond to time and azimuthal averages at the same radial location, $r = 10r_G$. (c): Points from the simulations of Machida & Matsumoto (2008) in the Paczyński-Wiita potential — triangle: High temperature case; square: Low temperature case. (d): Points from the simulations of Fragile & al. (2007) in Schwarzschild (dots) and $a = 0.9$ Kerr (crosses) spacetimes.

The constant \mathcal{L}_0 is defined by $\mathcal{L}_0 \equiv \eta \mathcal{L}_K(r_{ms})$. For the “hydrodynamical” case, the function $\mathcal{L}_{ms}(r)$ is constant,

$$\mathcal{L}_{ms}(r) = \mathcal{L}_0 [\mathcal{L}_K(r_{ms})/\mathcal{L}_0]^\beta = \text{const}, \quad (20)$$

while for the “MHD” case its is calculated from the $\Omega(r) = \Omega_K(r_{ms}) = \text{const}$ condition,

$$\mathcal{L}_{ms}(r) = -\frac{\Omega_{ms} g_{\phi\phi}(r, \pi/2) + g_{t\phi}(r, \pi/2)}{\Omega_{ms} g_{t\phi}(r, \pi/2) + g_{tt}(r, \pi/2)}. \quad (21)$$

Thus, there are only *three* dimensionless parameters in the model: (β, γ, η) . Their ranges are,

$$0 \leq \beta \leq 1, \quad -1 \leq \gamma \leq 1, \quad 1 \leq \eta \leq \eta_{max}. \quad (22)$$

The function $\mathcal{L}_K(r)$ is the Keplerian angular momentum in the equatorial plane, $\theta = \pi/2$, which for the Kerr metric is described by formula (5) and $\eta_{max} = \mathcal{L}_K(r_{mb})/\mathcal{L}_K(r_{ms})$. An equipressure surface that starts from the cusp is marginally bound for $\beta = 0$, $\gamma = 0$ and $\eta = \eta_{max}$.

4.3. Angular momentum on the equatorial plane

On the equatorial plane, $\sin \theta = 1$, and therefore only β and η (through \mathcal{L}_0) enter the distribution formulae (19).

$$\mathcal{L}(r, \pi/2) = \begin{cases} \mathcal{L}_0 \left(\frac{\mathcal{L}_K(r)}{\mathcal{L}_0} \right)^\beta & \text{for } r \geq r_{ms} \\ \mathcal{L}_{ms} & \text{for } r < r_{ms} \end{cases} \quad (23)$$

When $\beta = 0$, the angular momentum is constant, $\mathcal{L} = \mathcal{L}_0$, and when $\beta = 1$, it equals the Keplerian one, $\mathcal{L} = \mathcal{L}_K$.

For small values of β the assumed equatorial plane angular momentum (23) reproduces the characteristic shape, shown in Figure 2, which has been found in many numerical simulations of accretion flows — including stationary, axially symmetric, α viscosity, hydrodynamical “slim disks” (e.g. Abramowicz & al. 1988), and more recent, fully 3-D, non-stationary MHD simulations (e.g. Machida & Matsumoto 2008; Fragile & al. 2008). It corresponds to a distribution that is slightly sub-Keplerian for large radii, and closer to the black hole it crosses the Keplerian distribution twice, at $r_{center} > r_{ms}$ and at $r_{cusp} < r_{ms}$, forming a super-Keplerian part around r_{ms} . For $r < r_{cusp}$ the angular momentum is almost constant.

4.4. Angular momentum off the equatorial plane

Numerical simulations show that away from the equatorial plane, the angular momentum falls off. Figure 2 shows that indeed several MHD simulations (Machida & Matsumoto 2008; Fragile & al. 2008, Figure 2c and 2d respectively), feature a drop of angular momentum away from the equatorial plane. This behavior is reflected by the term $\sin^{2\gamma} \theta$ in (19). One may see that this form accurately mimics the outcome of the numerical simulations. Proga & Begelman (2003a,b) also studied axisymmetric accretion flows with low specific angular momentum using numerical simulations. In their inviscid hydrodynamical case Proga & Begelman (2003a) found that the inner accretion flow settles into a pressure-rotation supported torus in the equatorial region and a nearly radial inflow in the polar funnels. Furthermore, the specific angular momentum in the equatorial torus was nearly constant. This behavior changes once magnetic fields are introduced, as shown in Proga & Begelman (2003b). In the MHD case, the magnetic fields transport specific angular momentum so that in the innermost part of the flow, rotation is sub-Keplerian, whereas in the outer part, it is nearly Keplerian. Similar rotational profiles are also found in MHD simulations of the collapsar model of gamma-ray bursts (Proga & al. 2003; Baiotti & al. 2008), which use a sophisticated equation of state and neutrino cooling (instead of a simple adiabatic equation of state). Therefore, it appears that the rotational profile assumed in our model is quite robust as it has been obtained in a number of numerical experiments with various microphysics.

5. Results

Figures 3 and 4 show sequences of models calculated with the new ansatz (19) for black-hole spins $a = 0$ and 0.5, respectively. For these models we hold $\eta = \eta_{max}$ fixed, while β and γ are varied over the limits of their accessible ranges.

5.1. Equipressure surfaces on the axis of rotation

Figures 3 and 4 show an interesting change of the behavior of equipressure surfaces close to the axis with increasing γ . No equipressure surface can cross the symmetry axis when the de-

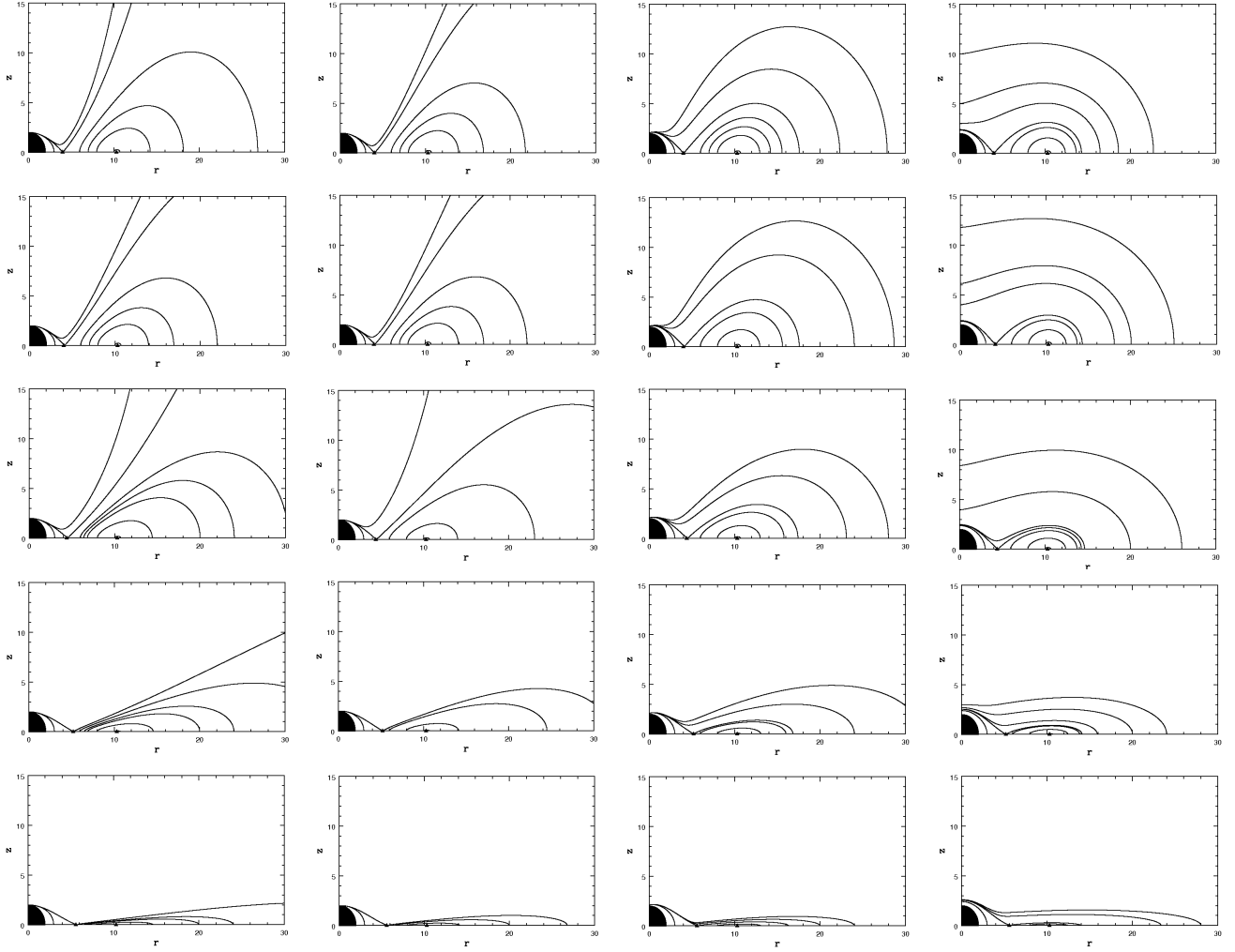


Fig. 3. Equipressure surfaces for $a = 0$ and $\eta = \eta_{max} = 1.085$. Five rows correspond to $\beta = (0.0), (0.1), (0.5), (0.9), (0.99)$ from the top to the bottom. Four columns correspond to $\gamma = (0.0), (0.1), (0.5), (0.9)$ from the left to the right. The upper left corner shows a “standard” Polish doughnut. The lower right corner shows an almost Keplerian disk at the equatorial plane, surrendered by a very low angular momentum envelope.

pendence of the angular momentum on θ is weak. This is the case for the first three columns of Figure 3 where $\gamma \leq 0.5$. On the other hand, for the angular momentum distributions with higher γ the equipressure surfaces cross the axis perpendicularly. This happens in plots of the last column of Figure 3. This behavior can be understood easily from the limit of $rd\theta/dr$ as $\theta \rightarrow 0$. In Schwarzschild spacetime equations (17) and (18) give

$$\lim_{\theta \rightarrow 0^+} \frac{rd\theta}{dr} = -\frac{2\mathcal{L}_k^2(r)}{\mathcal{L}^2(r, \pi/2)} \lim_{\theta \rightarrow 0^+} (\sin^{4\gamma-3} \theta). \quad (24)$$

The limit on the right-hand side is either 0, 1 or ∞ , depending on the value of γ . When $\gamma < 3/4$, $rd\theta/dr = 0$ and no equipressure surface goes across the axis. On the other hand, when $\gamma > 3/4$ equipressure surfaces cross the axis perpendicularly. Of course, a stationary torus may exist only within an equipotential surface located inside the Roche lobe, i.e., the critical self-crossing equipotential within the cusp (Abramowicz 1985).

5.2. Comparison with numerical simulations

Figure 5 illustrates that the results of the analytic models are well matched with results of modern 3-D MHD numerical simula-

tions (here taken from Fragile & al. 2007, 2008). For the correct choice of parameters, the model can reproduce many of the relevant features of the numerical results, including the locations of the cusp and pressure maximum, as well as the vertical thickness of the disk. At this stage, such qualitative agreement is all that can be hoped for. One notable difference between the analytic and numerical solutions is the behavior inside the cusp. While the analytic equipressure surfaces formally diverge toward the poles, the numerical solution maintains a fairly constant vertical height, which is also evident in Figure 1. This is because in the region inside the cusp, our assumption (10) about the form of the velocity is not valid — velocity cannot be consistent with a pure rotation only, $u^i = (u^t, u^\phi, 0, 0)$. In this region the radial velocity u^r must be non-zero and large. Thus, accuracy of our analytic models may only be trusted in the region outside the cusp, $r > r_{cusp}$.

6. Discussion

In this paper we assumed a form of the angular momentum distribution (19) and from this calculated the shapes and locations of the equipressure surfaces. This may be used in calcu-

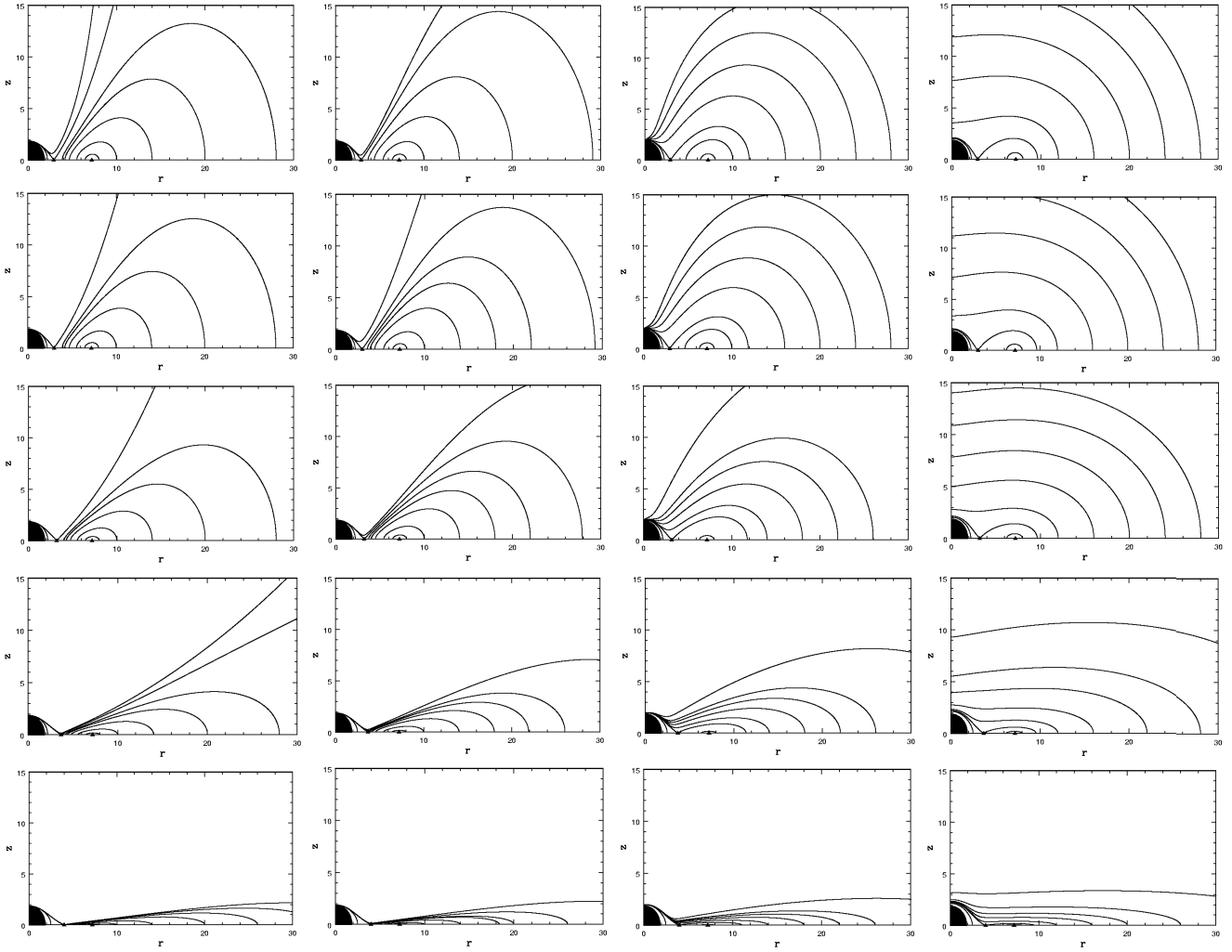


Fig. 4. Equipressure surfaces for $a = 0.5$ and $\eta = \eta_{\max} = 1.079$. Five rows correspond to $\beta = (0.0), (0.1), (0.5), (0.9), (0.99)$ from the top to the bottom. Four columns correspond to $\gamma = (0.0), (0.1), (0.5), (0.9)$ from the left to the right. The upper left corner shows a “standard” Polish doughnut. The lower right corner shows an almost Keplerian disk at the equatorial plane, surrendered by a very low angular momentum envelope.

lating spectra (in the optically thick case) by the same “surface” method as used in works by Sikora (1971) and Madau (1988).

We plan to construct the complete physical model of the interior in the second paper of this series. Here, we only outline the method by considering a simplified toy model. Let us denote $\rho = \epsilon + p$. We assume a toy (non-barytropic) equation of state and an entropy distribution, by writing,

$$p = e^{K(S)} \rho, \quad K = K(r, \theta). \quad (25)$$

Let us, in addition, define two functions connected to the entropy distribution,

$$\partial_\theta K = \kappa(r, \theta), \quad \frac{\partial_r K}{\partial_\theta K} = \lambda(r, \theta), \quad (26)$$

From the obvious condition that the second derivative commutator of pressure vanishes, $(\partial_r \partial_\theta - \partial_\theta \partial_r) p = 0$, and equations (25), (26) and (17) one derives,

$$\kappa = -\frac{\partial_r G_\theta - \partial_\theta G_r}{G_r - \lambda G_\theta}, \quad (27)$$

where G_r and G_θ are defined as

$$G_i(r, \theta) = \frac{\partial_i p}{\rho} \quad (28)$$

and can be calculated from the angular momentum distribution using equation (14). From (27) it is obvious that one cannot independently assume the functions $\kappa(r, \theta)$ and $\lambda(r, \theta)$ ⁴. Assuming $\lambda(r, \theta)$ is equivalent with assuming the shapes of isentropic surfaces. Indeed, from (26) one concludes that the function $\theta = \theta_S(r)$ that describes an isentropic surface is given by the equation,

$$\left[\frac{d\theta}{dr} \right]_S = -\lambda(r, \theta). \quad (29)$$

that may be directly integrated. Then the condition (27) gives the physical spacing (“labels”) to the isentropic surfaces, and through the equation of state (25) also to equipressure surfaces and isopicnic ($\rho = \text{const}$) surfaces.

Note, that a possible choice $\lambda = G_r/G_\theta$ corresponds, obviously, to the “von Zeipel” case in which equipressure and isentropic surfaces coincide. In this case the denominator in (27)

⁴ A somewhat similar situation in the case of rotating stars is known as the von Zeipel paradox (Tassoul 1978): *Pseudo-barytropic models in a state of permanent rotation cannot be used to describe rotating stars in strict radiative equilibrium.*

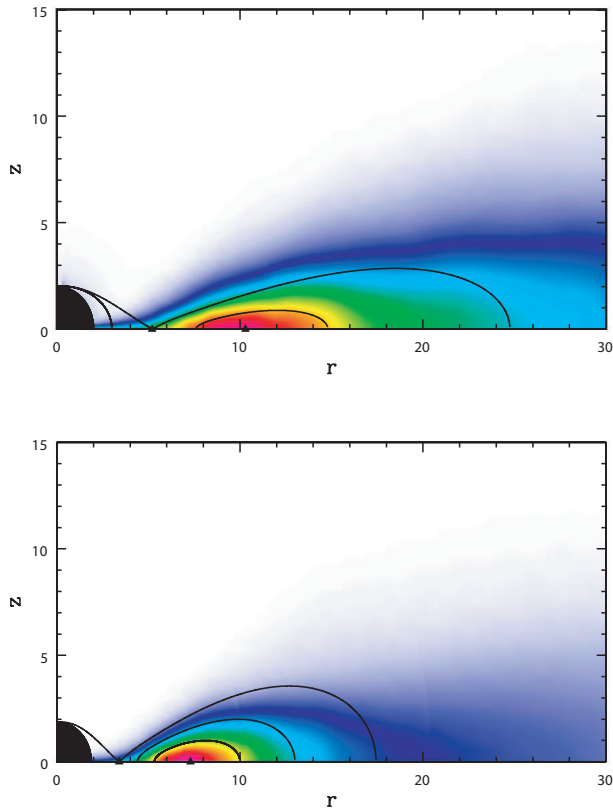


Fig. 5. Comparison of pressure distributions between the analytic model (*dark lines*) and numerical simulations (*colors*). The results of MHD simulations (taken from Fragile & al. 2007, 2008) have been time-averaged over one orbital period at $r = 25r_G$. *Upper panel:* Schwarzschild black hole ($a = 0$); the analytic model parameters are $\eta = 1.085$, $\beta = 0.9$, and $\gamma = 0.18$. *Lower panel:* Kerr black hole ($a = 0.5$); the analytic model parameters are $\eta = 1.079$, $\beta = 0.7$, and $\gamma = 0.2$.

vanishes, implying a singularity unless the numerator also vanishes. The condition for the numerator to vanish is, however, equivalent to the von Zeipel condition.

7. Conclusions

The new ansatz (19) captures two essential features of the angular momentum distribution in black hole accretion disks:

1. On the equatorial plane and far from the black hole, the angular momentum in the disk differs only little from the Keplerian one being slightly sub-Keplerian, but closer in it becomes (slightly) super-Keplerian and still closer, in the plunging region, sub-Keplerian again and nearly constant.
2. Angular momentum may significantly decrease off the equatorial plane, and become very low (even close to zero, in a non-rotating “corona”).

Models of tori described here may be useful not only for accretion disks but also for tori that form in the latest stages of neutron star binary mergers. This is relevant for gamma ray bursts (Witt & al. 1994) and gravitational waves (Baiotti & al. 2008).

Acknowledgements. We thank Daniel Proga and Luciano Rezzolla for helpful comments and suggestions. Travel expenses connected to this work were supported by the China Scholarship Council (Q.L.), the Polish Ministry of Science grant N203 0093/1466 (M.A.A.), and the Swedish Research Council grant VR Dnr 621-2006-3288 (P.C.F.).

References

- Abramowicz M.A., 1970, *Ap. Lett.* **7**, 73
 Abramowicz M.A., 1971, *Acta Astr.*, **21**, 81
 Abramowicz M.A., 1981, *Nature*, **294**, 235
 Abramowicz M.A., 1985, *PASJ*, **37**, 727
 Abramowicz M.A., 2005, *Astr. Nacht.* **326**, a collection of articles on the twin, high frequency QPOs
 Abramowicz M.A., Czerny B., Lasota J.-P., 1988, *ApJ*, **332**, 646
 Abramowicz M.A., Chen X., Kato S., Lasota J.-P., & Regev O., 1988, *ApJ*, **438**, L37
 Abramowicz M.A., Chen X.-M., Granath, M. & Lasota J.-P., 1997, *ApJ*, **471**, 762
 Abramowicz M.A. & Fragile C.P. 2008, *Black hole accretion disks*, in preparation for the Living Reviews
 Abramowicz, M.A., Jaroszyński, M., & Sikora, M. 1978, *A&A*, **63**, 221
 Abramowicz, M.A., Calvani M. & Nobili L., 1980, *ApJ*, **242**, 772
 Baiotti L., Giacomazzo B., & Rezzolla L., 2008, *Phys. Rev. D*, **78**, 0804033
 Bardeen J.M., 1970, *ApJ*, **162**, 71
 Blaes O.M., 1987 *MNRAS*, **227**, 975
 Blaes O.M., Arras P., & Fragile P.C., 2006 *MNRAS*, **369**, 1235
 De Villiers, J.-P. & Hawley, J. F., 2003, *ApJ*, **592**, 1060
 Fabian A.C. & Vaughan S., 2003, *MNRAS*, **340**, L28
 Fragile P.C., Blaes O.M., Anninos P., & Salmonson J.D., 2007, *ApJ*, **668**, 417,
 Fragile P.C., Lindner C.C., Anninos P., & Salmonson J.D., 2008, to appear in *ApJ*
 Jaroszyński M., Abramowicz M.A. & Paczyński B., 1980, *Acta Astr.*, **30**, 1
 Frank J., King A. & Raine D., 2002, *Accretion Power in Astrophysics*, Cambridge University Press (3rd edition)
 Hawley, J. F., Balbus, S. A., & Stone, J. M., 2001, *ApJ*, **554**, 49
 Komissarov S., 2006 *MNRAS* **368**, 993
 Kozłowski M. & Abramowicz M.A. & Jaroszyński M. 1978, *A&A*, ,
 Machida M. & Matsumoto R. 2008, *PASJ*, **60**, 613
 Madau P., 1988, *ApJ*, **327**, 116
 Montero P.J., Rezzolla L., & Yoshida S., 2004, *MNRAS*, **354**, 1040
 Narayan R., Yi I., 1988, *ApJ*, **444**, 231
 Ostriker J., Bodenheimer P. & Lynden-Bell D., 1966, *Phys. Rev. Lett.*, **17**, 816
 Paczyński B., 1982, *Astr. Gesellschaft*, **57**, 27
 Paczyński B. & Wiita P., 1980, *A&A*, **88**, 23
 Proga, D. & Begelman, M. C., 2003a, *ApJ*, **582**, 69
 Proga, D. & Begelman, M. C., 2003, *ApJ*, **592**, 767
 Proga, D., MacFadyen, A. I., Armitage, P. J., & Begelman, M. C., 2003, *ApJ*, **599**, L5
 Rezzolla L., Yoshida S., & Zanotti O., 2003a, *MNRAS*, **344**, 978
 Rezzolla L., Yoshida S., Maccarone T.J., & Zanotti O., 2003b, *MNRAS*, **344**, L37
 Sądowski A., 2008, *ApJ*, submitted
 Shafee R., McClintock J.E., Narayan R., Davis S.W., Li L.-X., & Remillard R.A., 2007, *ApJ*, **636**, L113
 Shafee R., McKinney J.C., Narayan R., Tchekhovskoy A. Gammie C.F. & McClintock J.E., 2008, *ApJ*, **687**, L25
 Sikora M., 1971, *MNRAS*, **196**, 257
 Shakura N.I. & Sunyaev R.A., 1973, *A&A*, **24**, 337
 Szuszkiewicz E., Malkan M. & Abramowicz M.A., 1996, *ApJ*, **458**, 474
 Tassoul J.-L., 1978, *Theory of Rotating Stars*, Princeton University Press, Chapter 7.2
 Witt H.J., Jaroszyński M., Haensel P., Paczyński B., Wambsganss J., 1994, *ApJ*, **422**, 219